LANGMUIR

pubs.acs.org/Langmuir Article

Exploring the Interfacial Dynamics of Unilamellar and Multilamellar Cationic Liposomes on SiO_2 and Their Interactions with Membrane-Active Peptide

Published as part of Langmuir special issue "Highlighting Contributions from our Editorial Board Members in 2024".

Hyunhyuk Tae, Soohyun Park, Younghwan Choe, Chungmo Yang, and Nam-Joon Cho*

Cite This: *Langmuir* 2024, 40, 24761−24770 Read Online

ACCESS | Metrics & More | Article Recommendations | Supporting Information

ABSTRACT: Understanding the interplay between lipid assemblies and solid supports is crucial for advancing model membrane systems and biomedical applications. This study investigates the interfacial behaviors of unilamellar and multilamellar cationic liposomes on silicon dioxide and their interactions with a membrane-active AH peptide. Using QCM-D monitoring, unilamellar liposomes were found to rapidly form SLBs through one-step adsorption kinetics, whereas multilamellar liposomes exhibited slower adsorption. Further addition of liposomes caused fusogenic interactions with SLBs, where multilamellar liposomes formed more rigid lipid membranes. Upon AH peptide exposure, unilamellar-based lipid membranes showed higher susceptibility to structural transformations, achieving complete SLB formation, while multilamellar-based lipid membranes displayed reduced sensitivity and retained residual viscoelastic components, indicative of incomplete SLB formation. These findings underscore the significant influence of liposome lamellarity on their interfacial dynamics and peptide interactions, crucial for designing effective lipid-based delivery and sensing systems.

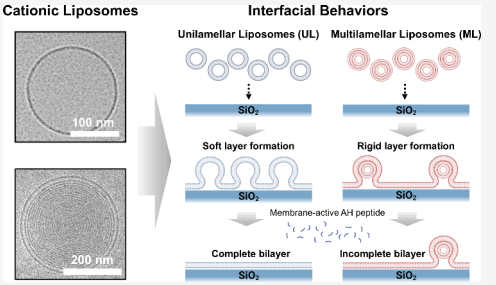

INTRODUCTION

Understanding the complex interplay between lipid assemblies and solid supports is crucial for comprehending the molecular dynamics of lipid bilayers and advancing model membrane systems like intact vesicle platforms and supported lipid bilayers (SLBs).[1−5] These interfacial insights into lipid assemblies not only shed light on fundamental biological processes at cellular membranes but also find practical applications in medical diagnostics, drug screening, and molecular interactions with biomolecules.[6−9]

Investigations in this field have extensively employed surface-sensitive techniques such as quartz crystal microbalance (QCM), surface plasmon resonance (SPR), atomic force microscopy (AFM), and total internal reflection fluorescence microscopy (TIRFM).[2,10−13] Among these, QCM presents notable benefits as a biosensor due to its compact and affordable instrumentation, high stability, and ability to provide real-time monitoring.[14−16] Recent advancements in QCM technology have further enhanced its capabilities. For instance, Murata et al. developed uniformly stacked flat DNA nanofilms on QCM sensors using the laser molecular beam deposition (LMBD) method, which outperforms DNA thin films fabricated by conventional spin coating.[17] Similarly, Zhou et al. created a wireless microelectromechanical systems (MEMS) QCM biosensor with an improved signal-to-noise ratio by embedding metallic micropillars through the glass substrates.[18] Additionally, the quartz crystal microbalance with dissipation monitoring (QCM-D) technique has proven valuable due to its high sensitivity to both mass changes and the viscoelastic properties of adsorbed layers, demonstrating its capabilities for investigating liposome adsorption, transformation, and biomolecular interactions on various substrates.[19,20]

The adsorption dynamics of liposomes onto solid substrates are influenced by various parameters, including lipid compositions,[21] temperature,[22] osmotic pressure,[23] liposome size,[5] and substrate properties.[2,24,25] These thermodynamic factors intricately govern the liposome−liposome and liposome−substrate interactions, controlling whether liposome adsorption occurs and, if so, whether the liposomes remain intact or undergo rupture. Nevertheless, the outcome of liposome adsorption is largely determined by the nature of the

Received: June 17, 2024
Revised: September 1, 2024
Accepted: September 5, 2024
Published: September 13, 2024

surfaces.[26,27] Under physiological conditions (e.g., pH 7.4), zwitterionic liposomes tend to self-assemble and form SLBs on substrates like glass, silicon oxide, and mica.[2,28] Conversely, when adsorbed on gold and titanium oxide, they remain intact without rupturing.[24,29] In support of this, Groves et al. demonstrated that certain oxide substrates serve as barriers to the SLB formation.[30,31] Additionally, Jackman et al. discovered that altering the pH or changing the solvent can modulate the hydration force on aluminum oxide, significantly impacting liposome adsorption and the formation of SLBs on this substrate.[3] On many substrates, silicon dioxide (SiO_2), by its hydrophilicity, optical transparency, and prevalence in electronics fabrication, is a commonly employed substrate for such investigations.[3,10,25] Previous research has demonstrated that modification of the membrane charge in liposomes by incorporating cationic or anionic phospholipids can alter the interaction between liposomes and SiO_2 surfaces, which subsequently affects the kinetics of SLB formation.[7] Biswas et al. further elucidated that the solution pH and the membrane surface charge significantly influence liposome adsorption behavior on SiO_2 by modulating the electrostatic and interfacial forces involved.[32] These studies underscore the pivotal role of membrane charge in governing the interfacial behaviors of liposomes.

Cationic liposomes, characterized by their positively charged lipid constituents, have emerged as a promising platform for various applications, including drug delivery, gene therapy, and surface modification.[33−35] For example, cationic liposomes utilizing the positively charged 1,2-dioleoyl-3-trimethylammonium-propane (DOTAP) lipid have been demonstrated for the ability to produce lipid bilayer coating on silica nanoparticles.[36,37] Moreover, cationic liposomes can form complexes with nucleic acids via electrostatic interactions and facilitate successful cellular delivery through membrane fusion by combining with fusogenic neutral lipids such as 1,2-dioleoyl-*sn*-glycero-3-phosphoethanolamine (DOPE).[38,39] Conventionally, cationic liposomes are prepared through extrusion or sonication techniques, resulting in predominantly unilamellar structures.[40,41] However, recent advancements in fabrication methods have introduced new possibilities to produce liposomes with unique attributes.[42] Notably, we have developed the liposome under cryoassembly (LUCA) cycle as a transformative technique that generates distinct cationic liposomes characterized by highly concentric multilamellar structures.[43] Such unique lamellar structure of liposomes can impact their adhesion to solid supports, as demonstrated that freeze−thaw pretreatment on zwitterionic liposomes facilitates the formation of planar bilayers on silicon oxide by encouraging the formation of unilamellar structures, irrespective of liposome size.[44] Consequently, the specific multilamellar architecture of cationic liposomes generated by the LUCA cycle may notably affect their interfacial interactions, which necessitates future investigation.

In this context, this study aims to compare the interfacial dynamics of both unilamellar and multilamellar cationic liposomes on SiO_2 and their interactions with the membrane-active peptide. Initially, the liposome formulation with distinct sizes and structures was assessed via dynamic light scattering (DLS) and cryogenic electron microscopy (cryo-EM). Subsequently, we employed a QCM-D instrument to monitor the adsorption and structural changes of liposomes on the SiO_2 surface in real time. Lastly, we investigated the interaction of these liposomes adhered to the SiO_2 surface with a membrane-active α-helical (AH) peptide, originating from the N-terminal amphipathic helix of the hepatitis C virus (HCV) NS5A protein and known for its ability to induce SLB formation by destabilizing adsorbed liposomes.[24,45] The AH peptide has been applied to various liposomes, including those containing cationic, anionic, and other biologically relevant lipids.[46,47] While the outer layer on multilamellar liposomes was revealed to be more prone to rupture by the AH peptide compared to unilamellar structures,[48] a deeper understanding of these interactions, particularly with positively charged multilamellar membranes, remains elusive. Therefore, the AH peptide was employed to modulate the structural dynamics of adhered cationic liposomes, and their interaction dynamics were comparatively explored.

EXPERIMENTAL SECTION

Reagents. 1,2-Dioleoyl-3-trimethylammonium-propane (chloride salt) (DOTAP) and 1,2-di(9*Z*-octadecenoyl)-*sn*-glycero-3-phosphoethanolamine (DOPE) dissolved in chloroform were obtained from Avanti Polar Lipids (Alabaster, AL). High-purity (96%) AH peptide (SGSWLRDVWDWICTVLTDFKTWLQSKL-NH_2) was synthesized by AnaSpec Corporation (Fremont, CA, USA). The lyophilized peptide was weighed and solubilized in deionized water to prepare a highly concentrated stock concentration (2 mg/mL). The molar concentration of the peptide was determined by absorbance measurements at 280 nm wavelength, and a Boeco-S220 spectrophotometer (Boeco, Hamburg, Germany) was used for the experiments.[49] The peptide concentration was 13 μM for all experiments in this study based on previous work that reported vesicle rupture in this peptide concentration range (13−15 μM).[24,45] The aqueous buffer used in all experiments was 10 mM tris(hydroxymethyl)-aminomethane (Tris) buffer containing 150 mM NaCl (pH 7.5), prepared using Milli-Q water (Millipore Sigma, Burlington, MA).

Liposome Preparation. Liposomes with net positive charge were fabricated by thin-film hydration, followed by extrusion or a LUCA cycle. First, the appropriate amounts of long-chain cationic DOTAP and neutral DOPE lipids in chloroform were added to a glass vial, and the solvent was evaporated by gentle drying under a stream of nitrogen gas and subsequent incubation in a vacuum desiccator overnight. Next, the dried lipid film was hydrated in Milli-Q-treated water or UltraPure DNase/RNase-free distilled water (Thermo Fisher Scientific, Waltham, MA) by vortexing. To prepare unilamellar liposomes, the resulting suspensions were extruded using track-etched polycarbonate filter membranes with a 400 nm diameter. To prepare multilamellar liposomes, the hydrated suspensions were subjected to five LUCA cycles, involving the following steps: (1) submerse in liquid nitrogen for 1 min, (2) thaw in a 60 °C water bath for 5 min, and (3) vortex for 30 s. The DOTAP and DOPE concentrations were fixed at 10 mM unless stated otherwise. Immediately before the QCM-D experiment, an aliquot of the stock lipid suspension was diluted 20-fold using the Tris buffer. The final DOTAP and DOPE concentrations in QCM-D were 0.25 mM, respectively.

Dynamic Light Scattering (DLS) Measurements. The size distribution was investigated using a 90Plus particle size/ζ PALS analyzer (Brookhaven Instruments Corporation, NY). For size distribution analysis, measurements were based on DLS at a scattering angle of 90° to minimize the reflection effect. The autocorrelation function was analyzed using the non-negative least-squares (NNLS) method. The NNLS method was utilized to generate the intensity-weighted curve of the liposome size distribution, and the polydispersity index (PDI) was calculated by $(\text{width/mean})^2$ for each population. To transform these intensity-weighted diagrams into number-weighted size distributions, one must account for the liposome mass as a function of the size. While this relationship is well-established for unilamellar liposomes, it is often uncertain for partially or predominantly multilamellar liposomes due to uncharacterized lamellarity. Consequently, we present only the original intensity-weighted size distribution curves. It is important to note

https://doi.org/10.1021/acs.langmuir.4c02273
Langmuir 2024, 40, 24761−24770

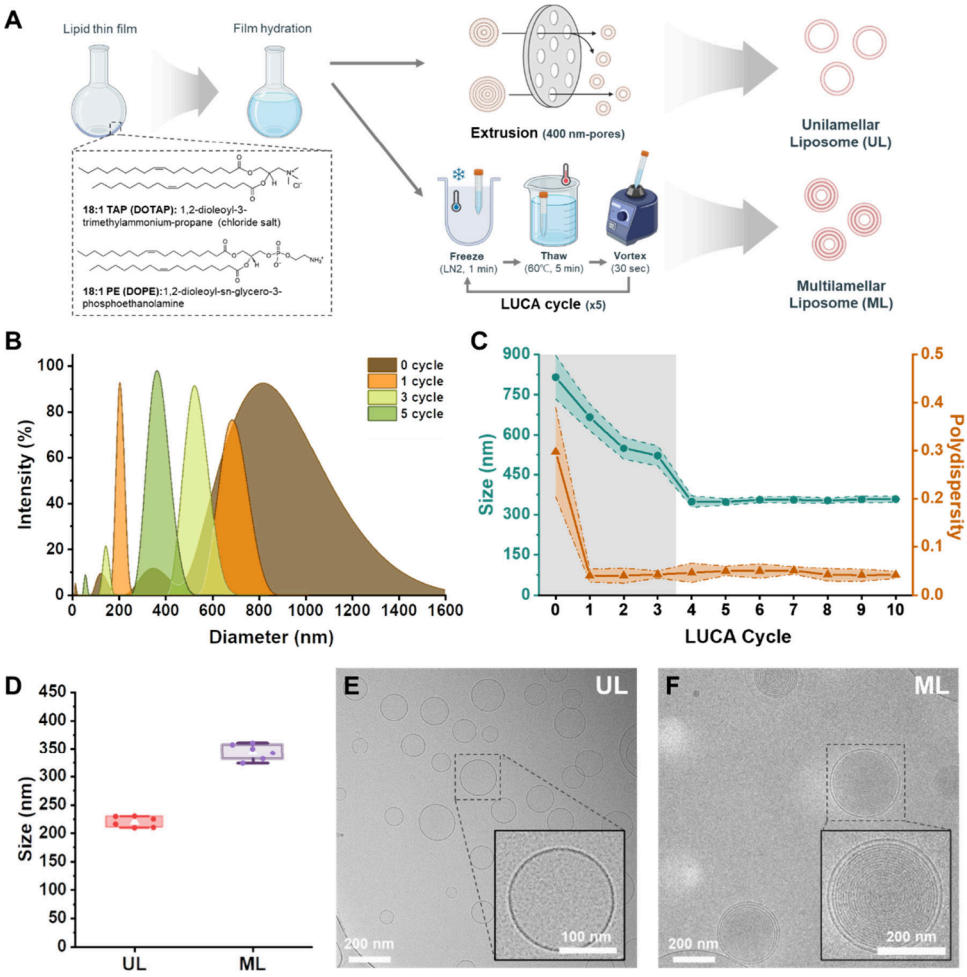

Figure 1. Fabrication of unilamellar (UL) and multilamellar (ML) cationic liposomes. (A) Schematics illustrating the methods for liposome fabrication with the chemical structures of the lipids utilized in this study. DOTAP is a permanently charged monocationic lipid, and DOPE is a neutral helper lipid promoting membrane fusion. UL was produced by extrusion through 400 nm pores, while ML was fabricated through five LUCA cycles, which is a precisely controlled freeze−thaw-based method. (B) Representative size distribution curves obtained from DLS in intensity-weighted mode for cationic liposomes treated with different numbers of LUCA cycles. (C) Effects of LUCA cycles on the mean diameter and polydispersity index of large-sized populations for cationic liposomes (n = 6, mean ± SD). The shaded gray area denotes the liposomes containing multiple size populations. (D) Mean diameters of UL and ML and (E, F) representative cryo-EM micrographs illustrating structural differences between them.

that in these curves the contribution of liposomes increases significantly with their size. Therefore, the actual relative proportion of larger liposomes is much smaller than that of their representation in intensity-weighted curves.

Cryogenic Electron Microscopy (Cryo-EM). To prepare samples for cryo-EM imaging, lacey carbon-coated 300 mesh copper grids (Electron Microscopy Sciences, Hatfield, PA) were glow discharged. Four microliters of sample solution was deposited onto a grid at 100% humidity, blotted with filter paper (2 s blotting time, 0 blot force), and plunged into liquid ethane (Vitrobot, FEI Company). Cryogrids were imaged by using a FEG 200 keV transmission electron microscope (Arctica, FEI Company) equipped with a direct electron detector (Falcon II, FEI Company). Images were recorded at a nominal 53 000× magnification with an integration time (exposure time) of 1 s.

Quartz Crystal Microbalance with Dissipation Monitoring (QCM-D). QCM-D experiments were conducted by using a Q-Sense E4 instrument (Biolin Scientific AB, Stockholm, Sweden). The quartz-crystal sensor chips had a fundamental frequency of 5 MHz, and the sensor surface had a 50 nm thick sputter-coated silicon dioxide layer. Before the experiment, the sensor chips were successively rinsed with 1% (w/v) sodium lauryl sulfate (SDS) solution, deionized water, and 95% ethanol, dried under a flow of nitrogen gas, and then treated in an oxygen plasma chamber (PDC-002, Harrick Plasma, Ithaca, NY) for 1 min. The temperature of the QCM-D chambers was maintained at 25 °C. All solutions were added under continuous flow conditions by using a peristaltic pump (Reglo Digital MS-4/6, Ismatec, Wertheim, Germany) at a flow rate of 50 μL/min. The Q-Soft software package (Biolin Scientific AB) was used to collect data at multiple odd overtones. Data processing was performed using Q-Tools (Biolin Scientific AB) and OriginPro (OriginLab, Northampton, MA) software programs.

RESULTS AND DISCUSSION

Fabrication of Unilamellar and Multilamellar Cationic Liposomes. We first characterized the biophysical properties of cationic liposomes fabricated using two different methods: extrusion and the LUCA cycle. Figure 1A illustrates the liposome preparation methods and expected structural differences between the unilamellar liposomes generated via extrusion and the multilamellar liposomes formed through the LUCA cycle. We chose extrusion as it is a conventional technique for generating unilamellar liposomes with monodisperse size distribution.[40] Conversely, the LUCA cycle was

https://doi.org/10.1021/acs.langmuir.4c02273
Langmuir 2024, 40, 24761−24770

applied to form the concentric multilamellar morphology in DOTAP/DOPE cationic liposomes, as demonstrated in our previous study.[43] For the lipid composition of the cationic liposomes, DOTAP and DOPE lipids were selected as the DOTAP/DOPE system has been commonly used for various applications.[39,50]

Upon hydration after thin-film formation, DLS analysis of cationic liposomes exhibited a broad size distribution with multimodal peaks at approximately 123, 345, and 815 nm, indicative of a heterogeneous population (Figure 1B). However, subjecting the liposomes to the LUCA cycle led to significant changes in the size distribution. After 1 cycle, the liposomes displayed two distinct peaks at 201 and 666 nm, suggesting that the LUCA cycle can effectively partition heterogeneous liposome populations into more defined size classes, albeit still exhibiting multiple degrees of size variability. Further refinement through 3 LUCA cycles resulted in a shift of the peaks to 141 and 520 nm, indicating that the repeated LUCA cycles promote the size reduction of liposomes. In addition, the size distribution of liposomes became more uniform by selectively concentrating the populations around 520 nm. Finally, after 5 LUCA cycles, the size distribution of the liposomes converged into a single peak at approximately 348 nm. This significant narrowing of the size distribution peak underscores the efficacy of the LUCA cycle in producing more homogeneous liposomes, which is crucial for applications requiring precise control over liposome dimensions and uniformity.

A similar trend was observed in the changes in average diameters and polydispersity index (PDI) in large liposome populations over the LUCA cycles (Figure 1C). Although the liposomes treated with from 0 to 3 LUCA cycles exhibited multimodal population distributions, the average diameters and PDI values of the largest size population can offer straightforward and valuable insights into their changes in response to the LUCA cycles.[51] Initially, the average diameter of cationic liposomes reduced from 810 ± 80 nm to 670 ± 50 nm in this population, accompanied by a decrease in PDI from 0.30 to 0.04 after 1 LUCA cycle, indicating the effect of the LUCA cycle on narrowing size distribution. While 1 LUCA cycle reduces the overall size distribution, it is important to note again that this process results in the partitioning of liposome populations into a multimodal distribution, as indicated by an increase in the relative error of the average size from 0.078 to 0.097 and illustrated by the distinct multimodal peaks observed in Figure 1B. The smaller population, approximately 201 nm, also displayed a narrow distribution with a PDI of 0.03, demonstrating the distinct size partitioning in well-defined size characteristics promoted by the LUCA cycle. Further treatments with up to 4 LUCA cycles induced a decrease in the average diameter of liposomes to 350 ± 20 nm with a uniform size distribution, evidenced by a PDI of 0.04. The decrease in mean diameter observed may be attributed not only to the overall reduction in the size of the majority of liposomes but also to a transition of some liposomes from larger to smaller size distributions, as depicted in Figure 1B. Given the importance of liposome size distribution in pharmaceutical fields, the uniform size distribution observed here provides a notable benefit, positioning the LUCA cycle as an effective method for creating lipid-based delivery systems.[43] Further LUCA cycles did not affect the average diameter or PDI of the liposomes. Based on these findings, 5 LUCA cycles were selected for further comparative analysis with the liposomes prepared by extrusion to investigate the structural differences of cationic liposomes.

The 400 nm extruded unilamellar liposomes (termed "UL") exhibited an average diameter of 220 ± 9 nm, while 5 LUCA cycled liposomes (termed "ML") showed a larger average diameter of 344 ± 15 nm (Figure 1D). Cryo-EM analysis revealed that UL consisted of unilamellar structures, demonstrating that the extrusion process effectively disrupted the multilamellar configurations in hydrated liposomes and resulted in the formation of relatively homogeneous unilamellar liposomes (Figure 1E). In contrast, the ML displayed a highly concentric multilamellar structure (Figure 1F). It is important to highlight that ML showed a distinctive onion-like architecture together with monodisperse size distribution. The formation of this distinctive structure might be influenced by the interactions of significant electrostatic charges in cationic lipids and external environments resulting from repeated phase transitions.[52,53] However, further investigation is necessary to fully comprehend this phenomenon. Collectively, these findings demonstrate that cationic liposomes with unilamellar and multilamellar structures can be successfully formulated by extrusion and the LUCA cycle, respectively.

Interfacial Behaviors of Unilamellar and Multilamellar Cationic Liposomes onto SiO_2. Next, we investigated the interfacial behavior of UL and ML on SiO_2 using QCM-D monitoring. QCM-D provides label-free detection of surface-specific kinetic analysis by measuring changes in resonance frequency (Δf) and energy dissipation (ΔD) in real-time, reflecting the mass and viscoelastic properties of the adsorbed layers, respectively. Therefore, this technique has been widely used to study the surface interactions of liposomes on solid surfaces.[25,54,55]

Upon injecting ULs onto SiO_2 (t = 7 min), the ULs were rapidly attached to the surface within 2 min, showing Δf changes of approximately −26 Hz (Figure 2A) and ΔD changes less than 1×10^{-6} (Figure 2C) (marked as step I). All overtones (n) exhibited similar value changes in step I (Figure S2A,C), demonstrating the formation of supported lipid bilayers (SLBs) while minimizing the adhesion of intact liposomes.[19,56] During SLB formation, ULs exhibited one-step adsorption kinetics and ruptured immediately upon adsorption, due to strong electrostatic forces between highly positively charged liposomes and negatively charged surface at pH 7.5 (marked as step I).[57,58] Once the SLBs were formed and additional ULs were introduced further, a significant decrease in Δf and an increase in ΔD were observed, along with the overtone-dependent signal changes in step II. Even though steps I and II were not sharply separated because of the continuous addition of liposomes, these changes suggest that extra ULs were either attached to or fused with the lipid bilayers, creating soft layers with viscoelastic properties due to the solvents within the intact/hemifused liposomes.[20] Although electrostatic repulsion is expected between the cationic SLBs and liposomes due to the positively charged DOTAP lipid, the intercalation behavior of ULs into SLBs appears to be facilitated by the presence of the fusogenic DOPE lipid. DOPE promotes membrane fusion by stabilizing negatively curved membrane surfaces, which are essential for the formation of fusion intermediates such as stalks and hemifusion states.[59,60] These intermediates are critical steps in the membrane fusion process, allowing ULs to integrate into the SLBs effectively, despite the electrostatic barriers posed by DOTAP. Consequently, mass uptake, observed by a decrease

https://doi.org/10.1021/acs.langmuir.4c02273
Langmuir 2024, 40, 24761−24770

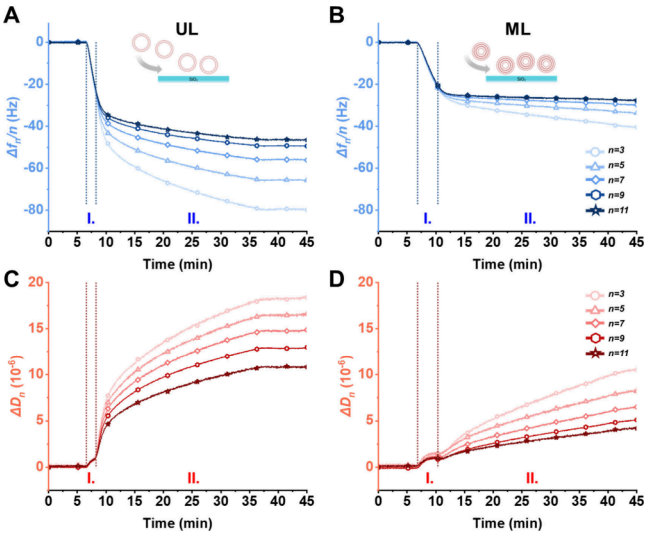

Figure 2. Adhesion of UL and ML onto the silicon dioxide surface. QCM-D tracked the change of resonance frequency for (A) UL and (B) ML adhesion and energy dissipation for (C) UL and (D) ML adhesion as a function of time from the 3rd to 11th overtone (n). The stable baseline in the buffer solution was first established, followed by the introduction of the liposomes into the measurement chamber at around t = 7 min. A washing step with the buffer solution was then conducted at around t = 37 min. I and II represent the one-step bilayer formation and further membrane fusion, respectively.

in Δf changes, reached saturation at approximately −79.6, −65.3, −55.9, −49.2, and −46.2 Hz for n = 3, 5, 7, 9, and 11, respectively. The increase in ΔD changes reached equilibrium at approximately 18.1 × 10^{-6}, 16.5 × 10^{-6}, 14.8 × 10^{-6}, 12.9 × 10^{-6}, and 10.7 × 10^{-6} for n = 3, 5, 7, 9, and 11, respectively.

Similar to ULs, MLs exhibited one-step adsorption behavior to form SLBs, as evidenced by the observed Δf changes of approximately −26 Hz (Figure 2B), and ΔD changes less than 1 × 10^{-6} (Figure 2D). However, the adsorption kinetics of MLs were notably slower compared to that of ULs (Figure S2B,D). This suggests that the multilayered structure of MLs requires more time to rupture and form SLB, in contrast to the unilamellar lipid membrane of ULs. The larger size of MLs might partially contribute to this effect, as larger liposomes experience greater steric hindrance, causing slower attainment of critical coverage of adsorbed liposomes compared to smaller liposomes.[61] Furthermore, the addition of extra MLs did not induce significant changes in Δf and ΔD during step II. This behavior can be attributed to the inherent rigidity of multilamellar lipid bilayers,[62,63] where the rigid structure of MLs likely leads to minimal changes in f and ΔD upon fusion into the SLBs, as well as a slower rupture process for SLB formation.

To further analyze the interfacial behaviors of ULs and MLs, we plotted time-independent Δf–ΔD curves based on the QCM-D measurements. The Δf values were plotted inversely on the x-axis to reflect a mass increase, while the ΔD values were plotted directly on the y-axis to represent changes in viscoelasticity. For ULs, the adsorption profile in step I exhibited a gentle slope for all overtones, likely because of the one-step adsorption and simultaneous rupture process to form SLBs (Figure 3A). MLs showed a slope similar to that of ULs in step I, demonstrating SLB formation by one-step adsorption kinetics (Figure 3B). In stage II, fusion-like behaviors were evident, characterized by a steeper and overtone-dependent slope compared to stage I for both ULs and MLs, suggesting a progressive structural transformation. The significant changes in Δf and ΔD intimate the presence of hemifused, not fully ruptured liposomes on SLBs for both ULs and MLs.

Two significant differences were noted between ULs and MLs at this stage. First, UL interactions with SLBs resulted in a considerable increase in both bound mass and viscoelasticity, as reflected by larger changes in Δf and ΔD, respectively, compared to MLs. This implies that ULs create soft, dynamic layers through membrane fusion, while MLs form more rigid structures due to the rigid multilamellar configuration, leading to smaller Δf and ΔD changes. Second, although the overall changes in Δf and ΔD were smaller for MLs, they exhibited a greater slope compared to that for ULs. This indicates a higher viscoelastic contribution of the adsorbed MLs relative to their mass, suggesting that MLs induce a faster structural transformation of the lipid membrane, likely due to their fusion behavior. This rapid fusion induced by the multilamellar structure of MLs has potential applications in drug delivery and sensing systems, warranting further investigation to fully understand the mechanism.

In summary, ULs create soft layers through fusion-like interactions with SLBs, whereas MLs, due to their inherent rigidity, form more stable and rigid structures. A hypothetical model illustrating their interactions with SiO_2 is presented in Figure 3C.

Interactions Dynamics between Cationic Liposomes on SiO_2 and Membrane-Active AH Peptide. To gain deeper insights into the impact of lamellar structures in cationic liposomes on biomolecular interactions, we employed the membrane-active AH peptide on cationic membrane

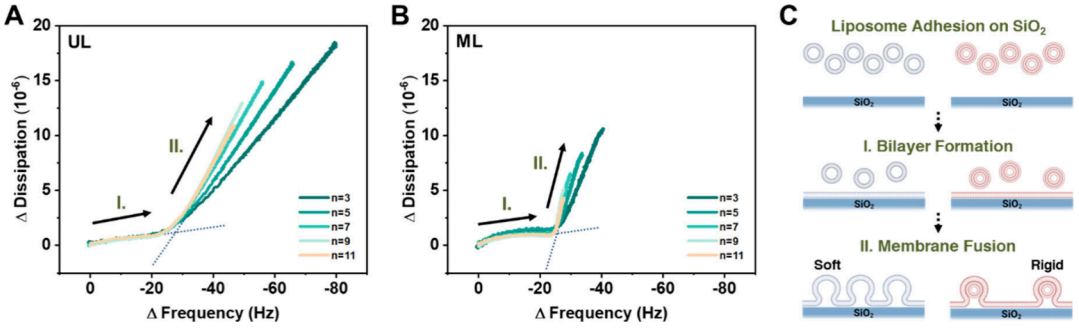

Figure 3. Frequency–dissipation (Δf–ΔD) plot for the (A) UL and (B) ML adhesion onto the silicon dioxide surface from the 3rd to 11th overtone (n), on the basis of the QCM-D experimental data from Figure 2. (C) Schematics illustrating the adhesion procedure of cationic liposomes onto silicon dioxide: (I) one-step lipid bilayer formation; (II) membrane fusion onto the bilayer promoted by fusogenic DOPE lipid.

https://doi.org/10.1021/acs.langmuir.4c02273
Langmuir 2024, 40, 24761−24770

surfaces formed by ULs and MLs (Figure 4A). The AH peptide has been known for its capability to disrupt the lipid

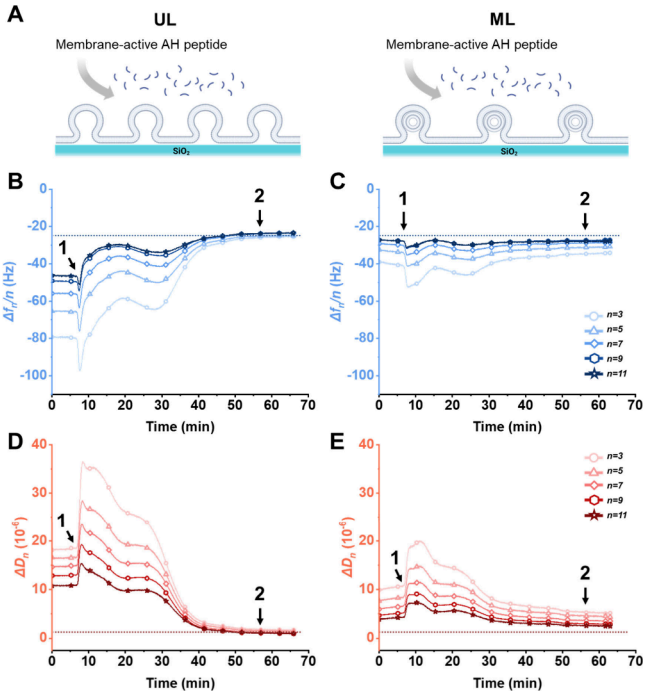

Figure 4. Interaction between membrane-active AH peptide and cationic liposomes adhered onto the silicon dioxide surface. (A) Schematics illustrating the treatment of AH peptide onto the absorbed cationic liposomes. QCM-D tracked the change of resonance frequency for peptide interaction with (B) UL and (C) ML, and energy dissipation for peptide interaction with (D) UL and (E) ML adhesion as a function of time from the 3rd to the 11th overtone (n). The peptide was introduced into the measurement chamber at around t = 7 min (arrow 1), followed by washing with the buffer solution at around t = 57 min (arrow 2). Note that the dashed lines in the graphs indicate the frequency and energy dissipation values associated with SLB formations.

envelopes of virus particles due to its amphipathicity (Figure S1).[45,64] Its membrane-active properties have been extensively studied in synthetic lipid membranes, where its distinctive characteristics facilitate the destabilization and rupture of adsorbed liposomes on solid supports, leading to the formation of planar lipid bilayers.[20,24] However, the interaction of the AH peptide with highly concentric multilamellar liposome structures remains unexplored.

Upon the addition of the AH peptide to the UL-derived lipid membranes (arrow 1), the initial binding of the AH peptide was observed, as indicated by the decrease in Δf (Figure 4B). This Δf shift is attributed to the peptide adsorption onto the liposomes and subsequent uptake in the hydrodynamically coupled solvent.[24,27] Following this, significant structural changes in the liposomes were detected, culminating in their rupture reflected by the Δf changes to approximately −26 Hz across all overtones. Consequently, the AH peptide induced a structural transformation of the adhered UL-based lipid membranes, leading to the formation of complete SLBs.

In contrast, ML-based lipid membranes exhibited a less sensitive response to the AH peptide injection, as reflected by the smaller Δf changes compared to those of UL-based lipid membranes (Figure 4C). This implies that multilamellar configurations are less susceptible to structural transformation by AH peptide. Ultimately, ML-based lipid membranes displayed overtone-dependent Δf shifts with additional mass uptake than typical Δf values for SLBs (~26 Hz), demonstrating that unruptured liposomes remained with coupled solvent even after AH peptide treatment.

The increase in hydration on lipid membranes following AH peptide addition was also reflected in the corresponding increase in ΔD shifts, but the changes in ΔD shifts were significantly higher for UL-based lipid membranes than for ML-based ones (Figure 4D,E). In UL-based lipid membranes, the final changes in ΔD shifts were less than 1×10^{-6}, consistent with previously reported value for SLB formation.[2] On the other hand, ML-based lipid membranes exhibited higher final values in ΔD shifts, suggesting incomplete SLB formations with unruptured liposomes.

To analyze the effect of lamellarity on the AH peptide-mediated liposomal structural transformation, time-independent Δf−ΔD curves were plotted (Figure 5). We identified five

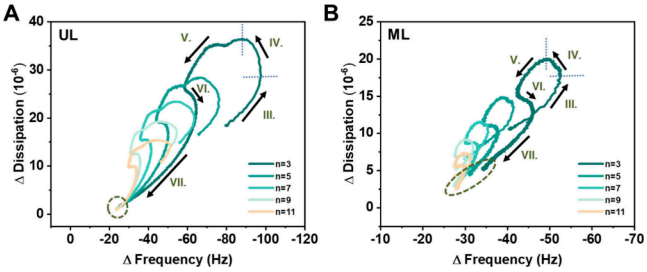

Figure 5. Structural transformation of cationic liposome induced by the AH peptide. The frequency−dissipation (f−D) curves were plotted for the (A) UL and (B) ML during the interaction between AH peptide and lipid membranes onto the silicon dioxide surface from the 3rd to 11th overtone (n), based on the QCM-D experimental data from Figure 4. Solid arrows labeled III−VII refer to five distinctly different processes during the whole measurement. Green dashed circles refer to the final values at different overtones.

distinct interaction processes between the AH peptide and liposomes, following (I) one-step lipid bilayer formation and (II) membrane fusion (see Figure 3). The main stages of interactions included (III) binding of AH peptide characterized by an increase in bound mass and energy dissipation, (IV) structural rearrangement of liposomes with a decrease in loaded mass and an increase in energy dissipation until reaching maximum value, (V−VII) liposome rupture and lipid relaxation with decreases in mass and energy dissipation. The interaction behaviors across these regimes were generally similar for both UL and ML-based lipid membranes.

Specifically, in stage III, the AH peptide was initially bound to the lipid membranes, as indicated by the increase in bound mass and energy dissipation until reaching the maximum Δf shift. These changes in Δf and ΔD were more pronounced in UL-based lipid membranes, suggesting that AH peptide binding and subsequent uptake of coupled solvent were more favored in softer UL-based lipid membranes. In stage IV, the liposomes on the lipid membranes underwent structural transformation until reaching the maximum ΔD shifts, while the bound mass decreased. These behaviors were generally observed by liposome swelling, presumably until reaching a threshold level.[27,65] Again, the changes in ΔD in this stage were less significant in ML-based lipid membranes, suggesting

https://doi.org/10.1021/acs.langmuir.4c02273
Langmuir 2024, 40, 24761−24770

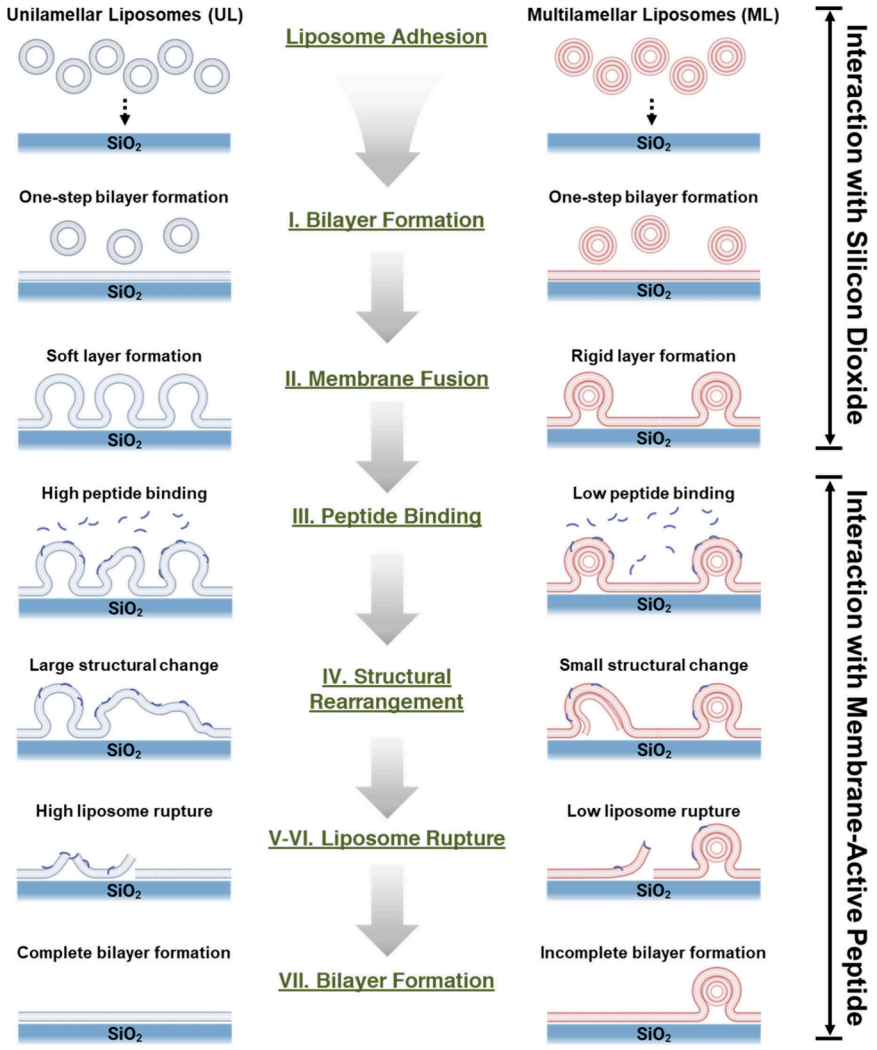

Figure 6. Schematic illustrations comparing the interfacial behavior of UL and ML on the silicon dioxide surface and their interactions with membrane-active AH peptide. UL exhibited the formation of soft lipid layers with higher increases in mass and viscoelasticity, while ML formed rigid lipid layers with smaller increases in mass and viscoelasticity. Upon binding with AH peptide, the UL-mediated lipid layers underwent significant structural changes, resulting in complete bilayer formation, whereas the ML-mediated lipid layers experienced minor structural changes, leading to incomplete bilayer formation.

that liposome swelling by the AH peptide was less preferred in ML-based lipid membranes.

Once the ΔD shifts reached their maximum values, the liposomes began to rupture in a stage (V). Notably, an interesting phenomenon was observed during liposome rupture for both UL and ML-based lipid membranes in stage (VI), where the additional mass was slightly loaded while the energy dissipation continued to decrease. Similar "zigzag" patterns have been observed with other membrane-active peptides.[66,67] This behavior might be attributed to the peptide insertion, with partial collapse of the lipid membrane. In this case, the decrease in ΔD shifts was more pronounced in lower overtones, indicating that the outer part of the lipid membrane became more rigid.[67] This is likely due to the rupture of the hemifused liposomes rather than structural rearrangements of pre-existing SLBs close to sensor surfaces. Consequently, liposomes continued to rupture until a planar bilayer was formed in a stage (VII) for UL-based lipid membranes. However, stage VII did not progress to SLB formation for ML-based lipid membranes (final values were marked as green dash circles in Figure 5), indicating the presence of residual viscoelastic components, presumably unruptured liposomes.

Taken together, AH peptide successfully facilitated SLB formation in cationic lipid layers derived from liposomes with unilamellar structures but not from liposomes with multilamellar structures. The lamellar structures in liposomes significantly influenced the interaction dynamics with the AH peptide, where UL-based lipid membranes exhibited higher susceptibility to AH peptide-induced structural transformations. These findings highlight the crucial role of lamellarity in the interactions of liposomes with membrane-active AH peptides. The overall interfacial behaviors of ULs and MLs are depicted in Figure 6.

CONCLUSIONS

This study elucidated how the lamellar structures of cationic liposomes influence their interfacial behavior on a silicon dioxide substrate and interactions with membrane-active AH peptides. QCM-D analysis demonstrated that unilamellar liposomes rapidly formed SLBs through one-step adsorption kinetics, whereas multilamellar liposomes exhibited slower

https://doi.org/10.1021/acs.langmuir.4c02273
Langmuir 2024, 40, 24761−24770

adsorption kinetics for SLB formations. Further addition of liposomes caused fusogenic interactions with SLBs, where multilamellar liposomes formed more rigid lipid membranes. Upon interaction with the membrane-active AH peptide, unilamellar-based lipid membranes displayed a higher susceptibility to peptide-induced structural transformations, leading to complete SLB formation. In contrast, multilamellar-based lipid membranes showed less sensitivity to the AH peptide, with residual viscoelastic components indicative of incomplete SLB formation.

Our findings underscore the crucial influence of liposome lamellarity on their interfacial dynamics and interactions with membrane-active peptides, highlighting the importance of structural characteristics in liposome applications. The differential behavior of unilamellar and multilamellar liposomes in forming SLBs and responding to membrane-active peptides has significant implications for the design and optimization of lipid-based delivery systems. For instance, unilamellar liposomes, with their rapid SLB formation and higher sensitivity to structural transformations, could be advantageous for applications requiring quick membrane fusion and the efficient delivery of therapeutic agents. Conversely, the rigidity and slower response of multilamellar liposomes might be beneficial in applications where more stable and sustained release profiles are desired such as in gene therapy or vaccine delivery. Moreover, the ability to manipulate the structural configuration of liposomes through techniques such as the LUCA cycle opens new avenues for tailoring liposome properties to specific biomedical applications. The insights gained from this study could also inform the development of biosensors and diagnostic platforms, where the dynamics of interaction between lipid membranes and peptides or other biomolecules are critical. Overall, this research provides a foundational understanding that could drive innovation in various fields, including drug delivery, gene therapy, biosensing, and beyond.

■ ASSOCIATED CONTENT

Supporting Information

The Supporting Information is available free of charge at https://pubs.acs.org/doi/10.1021/acs.langmuir.4c02273.

Helical wheel projection and QCM-D trends (PDF)

■ AUTHOR INFORMATION

Corresponding Author

Nam-Joon Cho − *School of Materials Science and Engineering, Nanyang Technological University, 639798, Singapore;* orcid.org/0000-0002-8692-8955; Email: njcho@ntu.edu.sg

Authors

Hyunhyuk Tae − *School of Materials Science and Engineering, Nanyang Technological University, 639798, Singapore;* orcid.org/0000-0002-0459-5879

Soohyun Park − *School of Materials Science and Engineering, Nanyang Technological University, 639798, Singapore;* orcid.org/0000-0003-3261-7585

Younghwan Choe − *School of Materials Science and Engineering, Nanyang Technological University, 639798, Singapore*

Chungmo Yang − *School of Materials Science and Engineering, Nanyang Technological University, 639798, Singapore*

Complete contact information is available at: https://pubs.acs.org/10.1021/acs.langmuir.4c02273

Notes

The authors declare the following competing financial interest(s): N.-J.C. is a co-inventor on U.S. Patent No. 8,728,793 which is related to the application of AH peptide molecules for antiviral therapy. The other authors declare no competing interests.

■ ACKNOWLEDGMENTS

This research was supported by the Ministry of Education (MOE) in Singapore under Grants RG111/20 and RG34/22. In addition, this work was supported by the National Research Foundation in Singapore (NRF) under Grant REQ414940. H.T. is supported by a SINGA graduate scholarship from the A*STAR Graduate Academy, Singapore. The LUCA Cycle is a proprietary technology developed by LUCA AICell Inc., with T. H. Kim being the credited inventor of this advanced processing method, for which a TD has been filed.

■ REFERENCES

(1) Tabaei, S. R.; Ng, W. B.; Cho, S.-J.; Cho, N.-J. Controlling the formation of phospholipid monolayer, bilayer, and intact vesicle layer on graphene. *ACS Appl. Mater. Interfaces* **2016**, *8*, 11875−11880.

(2) Keller, C.; Kasemo, B. Surface specific kinetics of lipid vesicle adsorption measured with a quartz crystal microbalance. *Biophys. J.* **1998**, *75*, 1397−1402.

(3) Jackman, J. A.; Tabaei, S. R.; Zhao, Z.; Yorulmaz, S.; Cho, N.-J. Self-assembly formation of lipid bilayer coatings on bare aluminum oxide: overcoming the force of interfacial water. *ACS Appl. Mater. Interfaces* **2015**, *7*, 959−968.

(4) Zan, G. H.; Jackman, J. A.; Kim, S.-O.; Cho, N.-J. Controlling lipid membrane architecture for tunable nanoplasmonic biosensing. *Small* **2014**, *10*, 4828−4832.

(5) Reimhult, E.; Höök, F.; Kasemo, B. Intact vesicle adsorption and supported biomembrane formation from vesicles in solution: influence of surface chemistry, vesicle size, temperature, and osmotic pressure. *Langmuir* **2003**, *19*, 1681−1691.

(6) Luchini, A.; Vitiello, G. Understanding the nano-bio interfaces: Lipid-coatings for inorganic nanoparticles as promising strategy for biomedical applications. *Front. Chem.* **2019**, *7*, 343.

(7) Jackman, J. A.; Cho, N.-J.; Duran, R. S.; Frank, C. W. Interfacial binding dynamics of bee venom phospholipase A2 investigated by dynamic light scattering and quartz crystal microbalance. *Langmuir* **2010**, *26*, 4103−4112.

(8) Pengo, P.; Şologan, M.; Pasquato, L.; Guida, F.; Pacor, S.; Tossi, A.; Stellacci, F.; Marson, D.; Boccardo, S.; Pricl, S.; Posocco, P. Gold nanoparticles with patterned surface monolayers for nanomedicine: current perspectives. *Eur. Biophys. J.* **2017**, *46*, 749−771.

(9) Fong, W.-K.; Negrini, R.; Vallooran, J. J.; Mezzenga, R.; Boyd, B. J. Responsive self-assembled nanostructured lipid systems for drug delivery and diagnostics. *J. Colloid Interface Sci.* **2016**, *484*, 320−339.

(10) Anderson, T. H.; Min, Y.; Weirich, K. L.; Zeng, H.; Fygenson, D.; Israelachvili, J. N. Formation of supported bilayers on silica substrates. *Langmuir* **2009**, *25*, 6997−7005.

(11) Dacic, M.; Jackman, J. A.; Yorulmaz, S.; Zhdanov, V. P.; Kasemo, B.; Cho, N.-J. Influence of divalent cations on deformation and rupture of adsorbed lipid vesicles. *Langmuir* **2016**, *32*, 6486−6495.

(12) Tabaei, S. R.; Jönsson, P.; Brändén, M.; Höök, F. Self-assembly formation of multiple DNA-tethered lipid bilayers. *J. Struct. Biol.* **2009**, *168*, 200−206.

(13) Reimhult, E.; Larsson, C.; Kasemo, B.; Höök, F. Simultaneous surface plasmon resonance and quartz crystal microbalance with dissipation monitoring measurements of biomolecular adsorption

events involving structural transformations and variations in coupled water. *Anal. Chem.* **2004**, *76*, 7211−7220.
(14) Chen, D.; Li, H.; Su, X.; Li, N.; Wang, Y.; Stevenson, A. C.; Hu, R.; Li, G. A wireless-electrodeless quartz crystal microbalance method for non-enzymatic glucose monitoring. *Sens. Actuators B: Chem.* **2019**, *287*, 35−41.
(15) Reviakine, I.; Johannsmann, D.; Richter, R. P. Hearing what you cannot see and visualizing what you hear: interpreting quartz crystal microbalance data from solvated interfaces. *Anal. Chem.* **2011**, *83*, 8838−8848.
(16) Ogi, H. Wireless-electrodeless quartz-crystal-microbalance biosensors for studying interactions among biomolecules: A review. *Proc. Jpn. Acad. Ser. B* **2013**, *89*, 401−417.
(17) Murata, T.; Minami, K.; Yamazaki, T.; Sato, T.; Koinuma, H.; Ariga, K.; Matsuki, N. Nanometer-flat DNA-featured thin films prepared via laser molecular beam deposition under high-vacuum for selective methanol sensing. *Bull. Chem. Soc. Jpn.* **2023**, *96*, 29−34.
(18) Zhou, L.; Kato, F.; Iijima, M.; Nonaka, T.; Kuroda, S. i.; Ogi, H. Mass-fabrication scheme of highly sensitive wireless electrodeless MEMS QCM biosensor with antennas on inner walls of microchannel. *Anal. Chem.* **2023**, *95*, 5507−5513.
(19) Cho, N.-J.; Kanazawa, K. K.; Glenn, J. S.; Frank, C. W. Employing two different quartz crystal microbalance models to study changes in viscoelastic behavior upon transformation of lipid vesicles to a bilayer on a gold surface. *Anal. Chem.* **2007**, *79*, 7027−7035.
(20) Cho, N.-J.; Wang, G.; Edvardsson, M.; Glenn, J. S.; Hook, F.; Frank, C. W. Alpha-helical peptide-induced vesicle rupture revealing new insight into the vesicle fusion process as monitored in situ by quartz crystal microbalance-dissipation and reflectometry. *Anal. Chem.* **2009**, *81*, 4752−4761.
(21) Dimitrievski, K.; Kasemo, B. Influence of lipid vesicle composition and surface charge density on vesicle adsorption events: a kinetic phase diagram. *Langmuir* **2009**, *25*, 8865−8869.
(22) Reimhult, E.; Höök, F.; Kasemo, B. Temperature dependence of formation of a supported phospholipid bilayer from vesicles on SiO 2. *Phys. Rev. E* **2002**, *66*, No. 051905.
(23) Jackman, J. A.; Choi, J.-H.; Zhdanov, V. P.; Cho, N.-J. Influence of osmotic pressure on adhesion of lipid vesicles to solid supports. *Langmuir* **2013**, *29*, 11375−11384.
(24) Cho, N.-J.; Cho, S.-J.; Cheong, K. H.; Glenn, J. S.; Frank, C. W. Employing an amphipathic viral peptide to create a lipid bilayer on Au and TiO2. *J. Am. Chem. Soc.* **2007**, *129*, 10050−10051.
(25) Cho, N.-J.; Jackman, J. A.; Liu, M.; Frank, C. W. pH-Driven assembly of various supported lipid platforms: A comparative study on silicon oxide and titanium oxide. *Langmuir* **2011**, *27*, 3739−3748.
(26) Florin, E.-L.; Gaub, H. Painted supported lipid membranes. *Biophys. J.* **1993**, *64*, 375−383.
(27) Cho, N.-J.; Frank, C. W.; Kasemo, B.; Höök, F. Quartz crystal microbalance with dissipation monitoring of supported lipid bilayers on various substrates. *Nat. Protoc.* **2010**, *5*, 1096−1106.
(28) Keller, C.; Glasmästar, K.; Zhdanov, V.; Kasemo, B. Formation of supported membranes from vesicles. *Phys. Rev. Lett.* **2000**, *84*, 5443.
(29) Reimhult, E.; Höök, F.; Kasemo, B. Vesicle adsorption on SiO 2 and TiO 2: dependence on vesicle size. *J. Chem. Phys.* **2002**, *117*, 7401−7404.
(30) Groves, J. T.; Ulman, N.; Boxer, S. G. Micropatterning fluid lipid bilayers on solid supports. *Science* **1997**, *275*, 651−653.
(31) Groves, J. T.; Ulman, N.; Cremer, P. S.; Boxer, S. G. Substrate−membrane interactions: mechanisms for imposing patterns on a fluid bilayer membrane. *Langmuir* **1998**, *14*, 3347−3350.
(32) Biswas, K. H.; Jackman, J. A.; Park, J. H.; Groves, J. T.; Cho, N.-J. Interfacial forces dictate the pathway of phospholipid vesicle adsorption onto silicon dioxide surfaces. *Langmuir* **2018**, *34*, 1775−1782.
(33) Vishwakarma, M.; Agrawal, P.; Soni, S.; Tomar, S.; Haider, T.; Kashaw, S. K.; Soni, V. Cationic nanocarriers: A potential approach for targeting negatively charged cancer cell. *Adv. Colloid Interface Sci.* **2024**, *327*, No. 103160.
(34) Liu, C.; Zhang, L.; Zhu, W.; Guo, R.; Sun, H.; Chen, X.; Deng, N. Barriers and strategies of cationic liposomes for cancer gene therapy. *Mol. Ther., Methods Clin. Dev.* **2020**, *18*, 751−764.
(35) Reinhardt, N.; Adumeau, L.; Lambert, O.; Ravaine, S.; Mornet, S. Quaternary ammonium groups exposed at the surface of silica nanoparticles suitable for DNA complexation in the presence of cationic lipids. *J. Phys. Chem. B* **2015**, *119*, 6401−6411.
(36) Dengler, E. C.; Liu, J.; Kerwin, A.; Torres, S.; Olcott, C. M.; Bowman, B. N.; Armijo, L.; Gentry, K.; Wilkerson, J.; Wallace, J.; et al. Mesoporous silica-supported lipid bilayers (protocells) for DNA cargo delivery to the spinal cord. *J. Controlled Release* **2013**, *168*, 209−224.
(37) Liu, J.; Jiang, X.; Ashley, C.; Brinker, C. J. Electrostatically mediated liposome fusion and lipid exchange with a nanoparticle-supported bilayer for control of surface charge, drug containment, and delivery. *J. Am. Chem. Soc.* **2009**, *131*, 7567−7569.
(38) Bailey, A. L.; Cullis, P. R. Membrane fusion with cationic liposomes: effects of target membrane lipid composition. *Biochemistry* **1997**, *36*, 1628−1634.
(39) Noguchi, A.; Furuno, T.; Kawaura, C.; Nakanishi, M. Membrane fusion plays an important role in gene transfection mediated by cationic liposomes. *FEBS Lett.* **1998**, *433*, 169−173.
(40) Lapinski, M. M.; Castro-Forero, A.; Greiner, A. J.; Ofoli, R. Y.; Blanchard, G. J. Comparison of liposomes formed by sonication and extrusion: rotational and translational diffusion of an embedded chromophore. *Langmuir* **2007**, *23*, 11677−11683.
(41) Zuidam, N. J.; Hirsch-Lerner, D.; Margulies, S.; Barenholz, Y. Lamellarity of cationic liposomes and mode of preparation of lipoplexes affect transfection efficiency. *Biochim. Biophys. Acta, Biomembr* **1999**, *1419*, 207−220.
(42) Shah, S.; Dhawan, V.; Holm, R.; Nagarsenker, M. S.; Perrie, Y. Liposomes: Advancements and innovation in the manufacturing process. *Adv. Drug Delivery Rev.* **2020**, *154*, 102−122.
(43) Tae, H.; Park, S.; Tan, L. Y.; Yang, C.; Lee, Y.-A.; Choe, Y.; Wüstefeld, T.; Jung, S.; Cho, N.-J. Elucidating Structural Configuration of Lipid Assemblies for mRNA Delivery Systems. *ACS Nano* **2024**, *18*, 11284−11299.
(44) Jackman, J. A.; Zhao, Z.; Zhdanov, V. P.; Frank, C. W.; Cho, N.-J. Vesicle adhesion and rupture on silicon oxide: Influence of freeze−thaw pretreatment. *Langmuir* **2014**, *30*, 2152−2160.
(45) Cho, N.-J.; Dvory-Sobol, H.; Xiong, A.; Cho, S.-J.; Frank, C. W.; Glenn, J. S. Mechanism of an amphipathic α-helical peptide's antiviral activity involves size-dependent virus particle lysis. *ACS Chem. Biol.* **2009**, *4*, 1061−1067.
(46) Zan, G. H.; Jackman, J. A.; Cho, N.-J. AH peptide-mediated formation of charged planar lipid bilayers. *J. Phys. Chem. B* **2014**, *118*, 3616−3621.
(47) Hardy, G. J.; Nayak, R.; Alam, S. M.; Shapter, J. G.; Heinrich, F.; Zauscher, S. Biomimetic supported lipid bilayers with high cholesterol content formed by α-helical peptide-induced vesicle fusion. *J. Mater. Chem.* **2012**, *22*, 19506−19513.
(48) Tabaei, S. R.; Cho, N.-J. Lamellar sheet exfoliation of single lipid vesicles by a membrane-active peptide. *Chem. Commun.* **2015**, *51*, 10272−10275.
(49) Edelhoch, H. Spectroscopic determination of tryptophan and tyrosine in proteins. *Biochemistry* **1967**, *6*, 1948−1954.
(50) Rädler, J. O.; Koltover, I.; Salditt, T.; Safinya, C. R. Structure of DNA-cationic liposome complexes: DNA intercalation in multilamellar membranes in distinct interhelical packing regimes. *Science* **1997**, *275*, 810−814.
(51) Woodbury, D. J.; Richardson, E. S.; Grigg, A. W.; Welling, R. D.; Knudson, B. H. Reducing liposome size with ultrasound: bimodal size distributions. *J. Liposome Res.* **2006**, *16*, 57−80.
(52) Whitesides, G. M.; Boncheva, M. Beyond molecules: Self-assembly of mesoscopic and macroscopic components. *Proc. Natl. Acad. Sci. U. S. A.* **2002**, *99*, 4769−4774.
(53) Elizondo, E.; Moreno, E.; Cabrera, I.; Córdoba, A.; Sala, S.; Veciana, J.; Ventosa, N. Liposomes and other vesicular systems:

https://doi.org/10.1021/acs.langmuir.4c02273
Langmuir 2024, 40, 24761−24770

structural characteristics, methods of preparation, and use in nanomedicine. *Prog. Mol. Biol. Transl. Sci.* **2011**, *104*, 1−52.
(54) Richter, R.; Mukhopadhyay, A.; Brisson, A. Pathways of lipid vesicle deposition on solid surfaces: a combined QCM-D and AFM study. *Biophys. J.* **2003**, *85*, 3035−3047.
(55) Reimhult, E.; Zäch, M.; Höök, F.; Kasemo, B. A multitechnique study of liposome adsorption on Au and lipid bilayer formation on SiO2. *Langmuir* **2006**, *22*, 3313−3319.
(56) Ohlsson, G.; Axelsson, P.; Henry, J.; Petronis, S.; Svedhem, S.; Kasemo, B. A miniaturized flow reaction chamber for use in combination with QCM-D sensing. *Microfluid. Nanofluidics* **2010**, *9*, 705−716.
(57) Cremer, P. S.; Boxer, S. G. Formation and spreading of lipid bilayers on planar glass supports. *J. Phys. Chem. B* **1999**, *103*, 2554−2559.
(58) Sut, T. N.; Jackman, J. A.; Cho, N.-J. Understanding how membrane surface charge influences lipid bicelle adsorption onto oxide surfaces. *Langmuir* **2019**, *35*, 8436−8444.
(59) Kawamoto, S.; Klein, M. L.; Shinoda, W. Coarse-grained molecular dynamics study of membrane fusion: Curvature effects on free energy barriers along the stalk mechanism. *J. Chem. Phys.* **2015**, *143*, No. 243112.
(60) Scheeder, A.; Brockhoff, M.; Ward, E. N.; Kaminski Schierle, G. S.; Mela, I.; Kaminski, C. F. Molecular Mechanisms of Cationic Fusogenic Liposome Interactions with Bacterial Envelopes. *J. Am. Chem. Soc.* **2023**, *145*, 28240−28250.
(61) Jackman, J. A.; Kim, M. C.; Zhdanov, V. P.; Cho, N.-J. Relationship between vesicle size and steric hindrance influences vesicle rupture on solid supports. *Phys. Chem. Chem. Phys.* **2016**, *18*, 3065−3072.
(62) Sagar, G. H.; Bellare, J. R. Estimation of mechanical strength of unilamellar and multilamellar AOT/water vesicles and their rupture using micropipet aspiration. *J. Phys. Chem. B* **2009**, *113*, 13805−13810.
(63) Vorselen, D.; Marchetti, M.; López-Iglesias, C.; Peters, P. J.; Roos, W. H.; Wuite, G. J. Multilamellar nanovesicles show distinct mechanical properties depending on their degree of lamellarity. *Nanoscale* **2018**, *10*, 5318−5324.
(64) Elazar, M.; Cheong, K. H.; Liu, P.; Greenberg, H. B.; Rice, C. M.; Glenn, J. S. Amphipathic helix-dependent localization of NS5A mediates hepatitis C virus RNA replication. *J. Virol.* **2003**, *77*, 6055−6061.
(65) Jackman, J. A.; Zan, G. H.; Zhdanov, V. P.; Cho, N.-J. Rupture of lipid vesicles by a broad-spectrum antiviral peptide: influence of vesicle size. *J. Phys. Chem. B* **2013**, *117*, 16117−16128.
(66) Lu, N.-Y.; Yang, K.; Li, J.-L.; Yuan, B.; Ma, Y.-Q. Vesicle deposition and subsequent membrane−melittin interactions on different substrates: A QCM-D experiment. *Biochim. Biophys. Acta, Biomembr* **2013**, *1828*, 1918−1925.
(67) McCubbin, G. A.; Praporski, S.; Piantavigna, S.; Knappe, D.; Hoffmann, R.; Bowie, J. H.; Separovic, F.; Martin, L. L. QCM-D fingerprinting of membrane-active peptides. *Eur. Biophys. J.* **2011**, *40*, 437−446.

https://doi.org/10.1021/acs.langmuir.4c02273
Langmuir 2024, 40, 24761−24770